Influence of the Ligand Structure of Hafnocene Polymerization Catalysts: A Theoretical Study on Ethene Insertion and Chain Propagation

Virve A. Karttunen,[†] Mikko Linnolahti,[†] Tapani A. Pakkanen,*[,†] John R. Severn,[‡] Esa Kokko,[‡] Janne Maaranen,[‡] and Päivi Pitkänen[‡]

Department of Chemistry, University of Joensuu, P.O. Box 111, FI-80101, Joensuu, Finland, and Borealis Polymers Oy, R&D, P.O. Box 330, FI-06101, Porvoo, Finland

Received January 17, 2008

The influence of the ligand structures of hafnocene polymerization catalysts on ethene insertion and chain propagation was systematically studied by quantum chemical methods. Altogether 54 hafnocenes were studied as a function of the ligand structures. Two consecutive ethene insertions and chain propagations were performed for the catalysts, giving rise to 15 intermediate structures along the reaction pathway. The behavior of the catalysts was analyzed as a function of ancillary ligands, ligand substituents, and bridging units. The differences along the reaction pathway are dominated by the changes in relative stabilities of the catalytic intermediate products. Large aromatic ancillary ligands and electron-donating ligand substituents strongly stabilize the catalyst cations. Steric effects introduced by the ligand framework mostly affect the feasibility of ethene π-coordination and the activation energy for chain propagation. The dominant effect of the relative stabilities of the catalyst intermediates sheds light on the catalytic performance of metallocenes, which may turn out to be useful in further catalyst development.

1. Introduction

Group 4 metallocenes are excellent catalysts for the polymerization of olefins. The single-site nature of the metallocene catalysts basically enables tailoring of the polymer properties, and hence detailed understanding of the polymerization mechanism is of great interest. While no mechanism has been explicitly proved correct, the Cossee−Arlman mechanism,[1] and its modifications to include agostic interactions,[2] is most widely accepted. Here, the inserted olefin monomer first forms a π-complex, followed by formation of a four-membered cyclic transition state. The resulting product with a propagated chain has a new coordination site available for the insertion of the next monomer.

The majority of the experimental and theoretical work on metallocene polymerization catalysts has focused on zirconocenes.[3] Recently, hafnocenes have attained increasing interest due to their bonding characteristics different from the zirconocenes.[4] On the other hand, the zirconocenes and hafnocenes are nearly isostructural, because of practically the same atomic radii of Zr and Hf.[5] There is plenty of polymerization data available for zirconocenes, but much less for hafnocenes. Nevertheless, the available data suggest that hafnocenes produce higher molecular weight polymers than zirconocenes.[3]

The previous theoretical studies on titanocenes and particularly on zirconocenes[6] provide useful guidelines for the study of hafnocenes. Due to the complexity of the polymerization system, not all influential factors can be included in the theoretical studies. In addition to the molecular structure of the catalyst itself, factors such as the cocatalyst, solvent, impurities, and reaction conditions have a pronounced effect on the polymerization process. The effect of the cocatalyst is particularly important, as it activates the catalyst precursor, and may have a role during the chain propagation and termination steps. Unfortunately, the structure of the most common cocatalyst, methylaluminoxane (MAO), has remained unsolved notwithstanding significant experimental and theoretical efforts.[7] The unknown structure of MAO has seriously handicapped the understanding of the polymerization process. To enlighten the

* To whom correspondence should be addressed. E-mail: tapani.pakkanen@joensuu.fi.

[†] University of Joensuu.

[‡] Borealis Polymers Oy.

(1) (a) Cossee, P. *J. Catal.* **1964**, *3*, 80. (b) Arlman, E. J. *J. Catal.* **1964**, *3*, 89. (c) Arlman, E. J.; Cossee, P. *J. Catal.* **1964**, *3*, 99.

(2) Brookhart, M.; Green, M. L. H.; Parkin, G. *PNAS* **2007**, *104*, 6908, and references therein.

(3) (a) Alt, H. G.; Köppl, A. *Chem. Rev.* **2000**, *100*, 1205.

(4) Marschner, C. *Angew. Chem., Int. Ed.* **2007**, *46*, 6770, and references therein.

(5) Cotton, F. A.; Wilkinson, G. *Advanced Inorganic Chemistry*, 3rd ed.; Wiley-Interscience: New York, 1972; p 927.

(6) (a) Jolly, C. A.; Marynick, D. S. *J. Am. Chem. Soc.* **1989**, *111*, 7968. (b) Prosenc, M. H.; Janiak, C.; Brintzinger, H. H. *Organometallics* **1992**, *11*, 4036. (c) Janiak, C. *J. Organomet. Chem.* **1993**, *452*, 63. (d) Weiss, H.; Ehrig, M.; Ahlrichs, R. *J. Am. Chem. Soc.* **1994**, *116*, 4919. (e) Fusco, R.; Longo, L. *Macromol. Theor. Simul.* **1994**, *3*, 895. (f) Woo, T. K.; Fan, L.; Ziegler, T. *Organometallics* **1994**, *13*, 432. (g) Woo, T. K.; Fan, L.; Ziegler, T. *Organometallics* **1994**, *13*, 2252. (h) Yoshida, T.; Koga, N.; Morokuma, K. *Organometallics* **1995**, *14*, 746. (i) Fan, L.; Harrison, D.; Woo, T. K.; Ziegler, T. *Organometallics* **1995**, *14*, 2018. (j) Lohrenz, J. C. W.; Woo, T. K.; Fan, L.; Ziegler, T. *J. Organomet. Chem.* **1995**, *497*, 91. (k) Lohrenz, J. C. W.; Woo, T. K.; Ziegler, T. *J. Am. Chem. Soc.* **1995**, *117*, 12793. (l) Stovneng, J. A.; Rytter, E. *J. Organomet. Chem.* **1996**, *519*, 277. (m) Cruz, V. L.; Munoz-Escalona, A.; Martinez-Salazar, J. *Polymer* **1996**, *37*, 1663. (n) Margl, P.; Deng, L.; Ziegler, T. *J. Am. Chem. Soc.* **1998**, *120*, 5517. (o) Margl, P.; Deng, L.; Ziegler, T. *Organometallics* **1998**, *17*, 933. (p) Thorshaug, K.; Stovneng, J. A.; Rytter, E.; Ystenes, M. *Macromolecules* **1998**, *31*, 7149. (q) Petitjean, L.; Pattou, D.; Ruiz-Lopez, M. F. *J. Phys. Chem. B* **1999**, *103*, 27. (r) Margl, P.; Deng, L.; Ziegler, T. *Top. Catal.* **1999**, *7*, 187. (s) Lanza, G.; Fragala, I. L.; Marks, T. J. *Organometallics* **2001**, *20*, 4006. (t) Talarico, G.; Blok, A. N. J.; Woo, T. K.; Cavallo, L. *Organometallics* **2002**, *21*, 4939. (u) Beddie, C.; Hollink, E.; Wei, P.; Gauld, J.; Stephan, D. W. *Organometallics* **2004**, *23*, 5240. (v) Ustynyuk, L.; Yu.; Fushman, E. A.; Razavi, A, *Kinet Catal.* **2006**, *47*, 213. (x) Jensen, V. R.; Koley, D.; Jagadeesh, M. N.; Thiel, W. *Macromolecules* **2005**, *38*, 10266.

10.1021/om800050d CCC: $40.75
Publication on Web 06/14/2008

situation, a few theoretical studies of chain propagation mechanisms for zirconocenes in the presence of proposed model structures of MAO have been reported.[8] Alternatively, other activators, such as the well-defined boron-based cocatalysts, can be used.[7a,9] Unlike MAO, the boron-based cocatalysts can also be employed in theoretical studies.[10]

Due to the complexity of the polymerization system, not all influential factors can be conveniently included in the theoretical studies at this time. The theoretical studies are currently most useful for obtaining qualitative trends, which can be helpful in catalyst development. With this in mind, we focus here on the effect of ligand structures of hafnocenes on insertion and chain propagation of ethene. The energetics of two consecutive ethene insertions and chain propagations are studied and analyzed as a function of the ligand structure, including various ancillary ligands, ligand substituents, and bridging units.

2. Computational Methods

All calculations were performed by the hybrid density functional B3LYP method.[11] For hafnium, Los Alamos ECP[12] (LANL2DZ) was employed, and the standard 6-31G* basis set for all other elements. The B3LYP/LANL2DZ 6-31G* level of theory has been previously demonstrated to produce reliable structures for hafnocenes.[13] All hafnocenes were fully optimized without any constraints. The true character of the transition states was confirmed by calculating harmonic frequencies,[14] showing exactly one imaginary frequency for each TS. The calculations were carried out with the Gaussian 03 program package.[15]

3. Results and Discussion

3.1. Choice of the Hafnocenes. The base for the studied set of hafnocenes is formed by experimentally characterized hafnocenes found from the Cambridge Structural Database. The hafnocenes were selected from the database with the following prerequisites: (a) exactly one Hf atom, (b) two cyclopentadienyl rings, (c) two chlorines as leaving groups, and (d) no transition metals other than Hf. The crystallographically characterized hafnocenes (C1−C39 in Figure 1) were supplemented with additional structures (H1−H15 in Figure 1) to enable direct comparison of the influence of a greater variety of structural modifications. Conformational analysis was carried out for the hafnocenes H1−H15 to locate the global minimum conformations. Altogether 54 hafnocenes were taken into the study, which is now referred as "the Hf-set". The same selection of "the Hf-set" was used in a preceding publication focusing on the activation step.[16]

3.2. Catalytic Intermediates along the Chain Propagation Pathway. The catalyst−ethene complex has a lot of structural freedom and can exist in several conformations. Hence, various polymerization routes, containing many different conformations, have been suggested for the metallocene-catalyzed ethene polymerization process. These reaction routes have been studied throughout for zirconocenes, but not for hafnocenes, and it is possible that there are differences in some cases. Using previous literature on zirconocenes as a guideline, we go through the intermediate structures of the polymerization routes for "the Hf-set".

The insertion of ethene can take place either from the front or back of the growing chain. Ziegler and co-workers recently concluded a back-side mechanism, where the chain does not rotate between the vacant sites, as the preferred mechanism for zirconocenes.[8a] Here we apply the back-side mechanism for a selected set of hafnocenes, but also take the conformations of the front-side insertion into account. Hence, the approach covers all the key structures of previously studied mechanisms. The studied catalytic intermediates, altogether 14, are illustrated in Figure 2 for a hafnocene with unsubstituted Cp ligands.

The results of all calculations are listed in Table 1. Relative energies (ΔE) reported in the tables and discussed in the text represent energy differences from the catalytic intermediates to the sum of the energies of the free cationic monomethyl forms and free ethene molecules. In this context, the cationic monomethyl form of hafnocene C1 is set as a reference structure ($\Delta E = 0$) for the other ligand structures to be compared with. Based on the results reported in Table 1, a summary of the ethene insertion and propagation pathways is given in the following. The main features along the pathway are summarized in Table 2.

Activation of the catalyst precursor produces the cationic monomethyl form, with a coordination site available for the ethene monomer. The study of the mechanism of the first ethene insertion is straightforward due to the absence of agostic interactions from the methyl group to the metal center.[6a–i,m,p,s] In terms of total energy, the ethene insertion is exothermic on average by 63 kJ/mol. Of the two π-complexes in the insertion

(7) Chen, E. Y.-X.; Marks, T. J. *Chem. Rev.* **2000**, *100*, 1391. (b) Zurek, E.; Ziegler, T. *Prog. Polym. Sci.* **2004**, *29*, 107. (c) Linnolahti, M.; Severn, J. R.; Pakkanen, T. A. *Angew. Chem., Int. Ed.* **2006**, *45*, 3331.

(8) (z) Zurek, E.; Ziegler, T. *Faraday Discuss.* **2003**, *124*, 93. (b) Belelli, P. G.; Castellani, N. J. *J. Mol. Catal A: Chem.* **2006**, *253*, 52.

(9) Pedeutour, J-N.; Radhakrishnan, K.; Cramail, H.; Deffieux, A. *Macromol. Rapid Commun.* **2001**, *22*, 1095.

(10) (a) Lanza, G.; Fragala, I. L.; Marks, T. J. *J. Am. Chem. Soc.* **1998**, *120*, 8257. (b) Chan, M. S. W.; Vanka, K.; Pye, C. C.; Ziegler, T. *Organometallics* **1999**, *18*, 4624. (c) Lanza, G.; Fragala, I. L.; Marks, T. J. *J. Am. Chem. Soc.* **2000**, *122*, 12764. (d) Vanka, K.; Chan, M. S. W.; Pye, C. C.; Ziegler, T. *Organometallics* **2000**, *19*, 1841. (e) Braga, D.; Grepioni, F.; Tedesco, E.; Calhorda, M. J. *Z. Anorg. Allg. Chem.* **2000**, *626*, 462. (f) Chan, M. S. W.; Ziegler, T. *Organometallics* **2000**, *19*, 5182. (g) Nifant'ev, I. E.; Ustynyuk, L. Y.; Laikov, D. N. *Organometallics* **2001**, *20*, 5375. (h) Schaper, F.; Geyer, A.; Brintzinger, H. H. *Organometallics* **2002**, *21*, 473. (i) Lanza, G.; Fragala, I. L.; Marks, T. J. *Organometallics* **2002**, *21*, 5594. (j) Vanka, K.; Xu, Z.; Ziegler, T. *Can. J. Chem.* **2003**, *81*, 1413. (k) Xu, Z.; Vanka, K.; Ziegler, T. *Organometallics* **2004**, *23*, 104. (l) Silanes, I.; Ugalde, J. M. *Organometallics* **2005**, *24*, 3233. (m) Ziegler, T.; Vanka, K.; Xu, Z. *C. R. Chim.* **2005**, *8*, 1552. (n) Ducere, J.-M.; Cavallo, L. *Organometallics* **2006**, *25*, 1431. (o) Sassmannshausen, J.; Track, A.; Dias, T. A. D. S. *Eur. J. Inorg. Chem.* **2007**, *16*, 2327.

(11) (a) Lee, C.; Yang, W.; Parr, R. G. *Phys. Rev. B.* **1988**, *37*, 785. (b) Becke, A. D. *J. Chem. Phys.* **1993**, *98*, 5648. (c) Stephens, P. J.; Devlin, F. J.; Chabalowski, C. F.; Frisch, M. J. *J. Phys. Chem.* **1994**, *98*, 11623.

(12) Hay, P. J.; Wadt, W. R. *J. Chem. Phys.* **1985**, *82*, 270.

(13) Karttunen, V. A.; Linnolahti, M.; Pakkanen, T. A.; Maaranen, J.; Pitkänen, P. *Theor. Chem. Acc.* **2007**, *118*, 899.

(14) (a) Peng, C.; Schlegel, H. B. *Isr. J. Chem.* **1993**, *33*, 449. (b) Peng, C.; Ayala, P. Y.; Schlegel, H. B.; Frisch, M. J. J. *Comput. Chem.* **1996**, *17*, 49.

(15) Frisch, M. J.; Trucks, G. W.; Schlegel, H. B.; Scuseria, G. E.; Robb, M. A.; Cheeseman, J. R.; Montgomery, J. A., Jr.; Vreven, T.; Kudin, K. N.; Burant, J. C.; Millam, J. M.; Iyengar, S. S.; Tomasi, J.; Barone, V.; Mennucci, B.; Cossi, M.; Scalmani, G.; Rega, N.; Petersson, G. A.; Nakatsuji, H.; Hada, M.; Ehara, M.; Toyota, K.; Fukuda, R.; Hasegawa, J.; Ishida, M.; Nakajima, T.; Honda, Y.; Kitao, O.; Nakai, H.; Klene, M.; Li, X.; Knox, J. E.; Hratchian, H. P.; Cross, J. B.; Bakken, V.; Adamo, C.; Jaramillo, J.; Gomperts, R.; Stratmann, R. E.; Yazyev, O.; Austin, A. J.; Cammi, R.; Pomelli, C.; Ochterski, J. W.; Ayala, P. Y.; Morokuma, K.; Voth, G. A.; Salvador, P.; Dannenberg, J. J.; Zakrzewski, V. G.; Dapprich, S.; Daniels, A. D.; Strain, M. C.; Farkas, O.; Malick, D. K.; Rabuck, A. D.; Raghavachari, K.; Foresman, J. B.; Ortiz, J. V.; Cui, Q.; Baboul, A. G.; Clifford, S.; Cioslowski, J.; Stefanov, B. B.; Liu, G.; Liashenko, A.; Piskorz, P.; Komaromi, I.; Martin, R. L.; Fox, D. J.; Keith, T.; Al-Laham, M. A.; Peng, C. Y.; Nanayakkara, A.; Challacombe, M.; Gill, P. M. W.; Johnson, B.; Chen, W.; Wong, M. W.; Gonzalez, C.; Pople, J. A. *Gaussian 03, Revision C.02*; Gaussian, Inc.: Wallingford, CT, 2004.

(16) Karttunen, V. A.; Linnolahti, M.; Turunen, A.; Pakkanen, T. A.; Severn, J. R.; Maaranen, J.; Kokko, E.; Pitkaenen, P. *J. Organomet. Chem.* **2008**, *693*, 155.

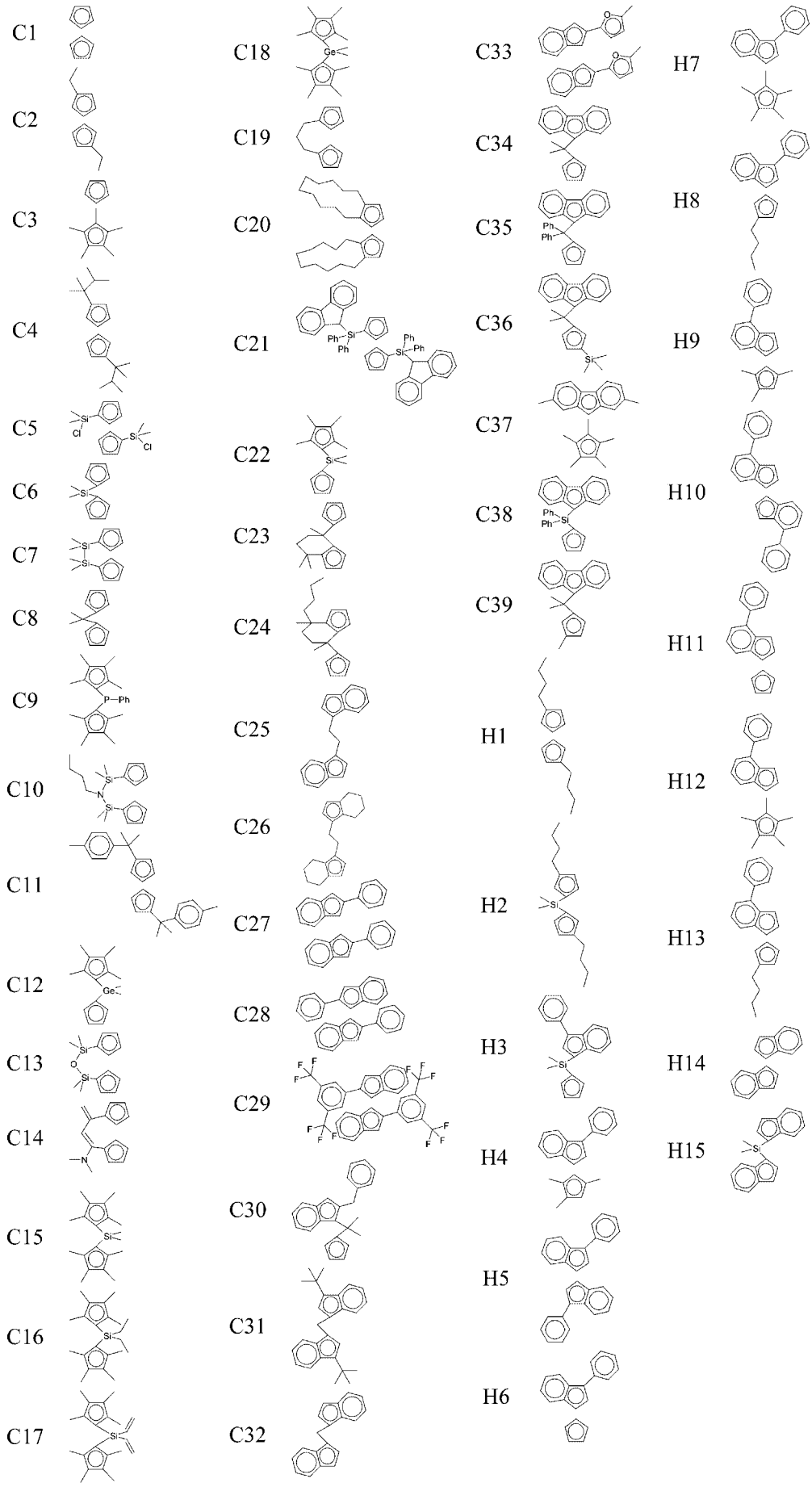

Figure 1. Schematic ligand structures of the studied hafnocenes.

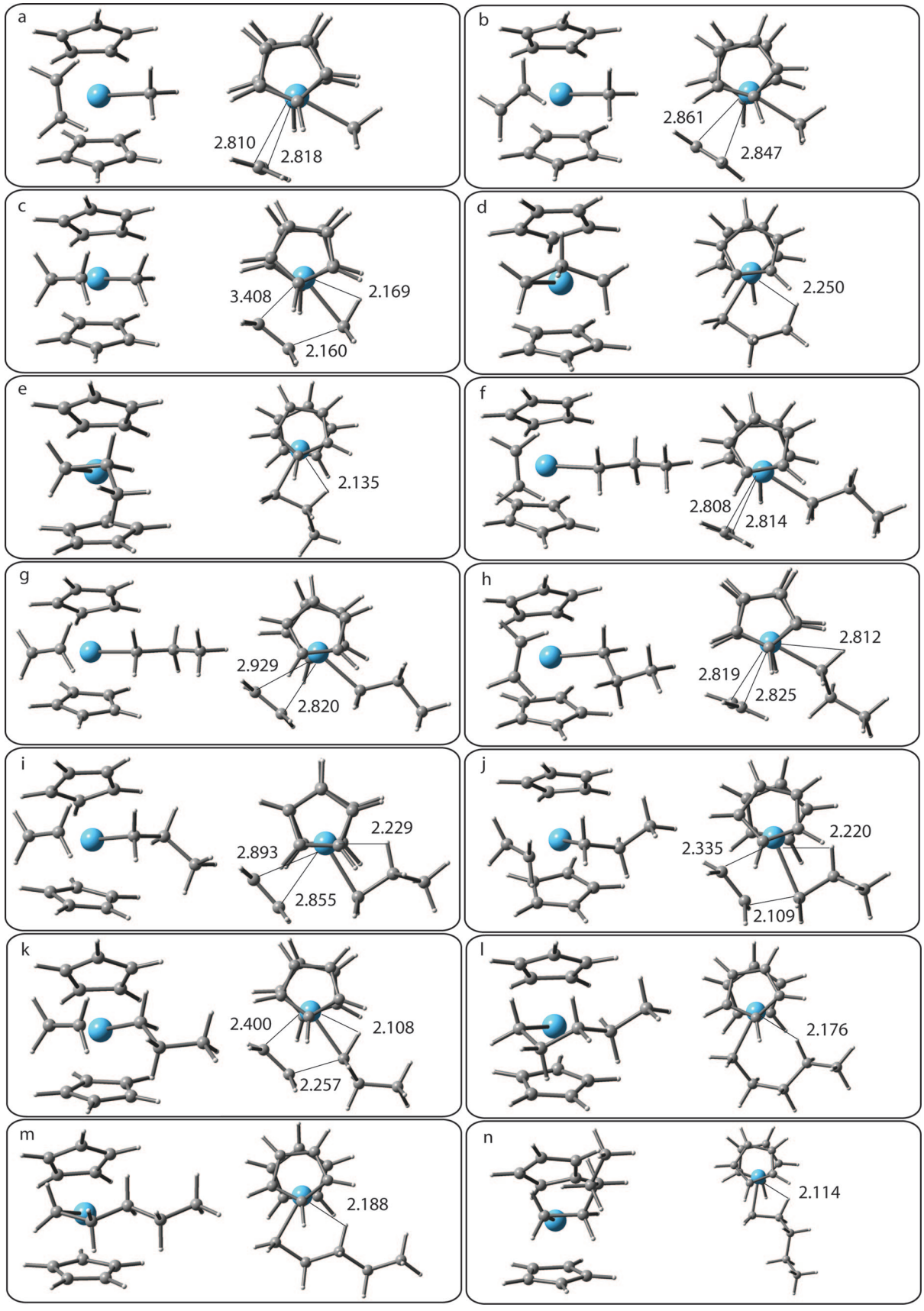

Figure 2. Front and top views of the studied catalytic intermediates for catalyst C1 (see Figure 1): (a) vertical π-complex, (b) horizontal π-complex, (c) α-agostic transition state, (d) γ-agostic propyl product, (e) β-agostic propyl product, (f) second vertical π-complex, (g) second horizontal π-complex, (h) second α-agostic π-complex, (i) second β-agostic π-complex, (j) second β-agostic transition state, (k) second α-agostic transition state, (l) δ-agostic pentyl product, (m) γ-agostic pentyl product, and (n) β-agostic pentyl product. The bond lengths are reported in angströms.

Table 1. Relative Energies (kJ/mol)[e] of the Catalytic Intermediates along the Reaction Pathway for "the Hf-Set"

				first ethene						second ethene					
hafnocene	cationic monomethyl	vertical π-complex (a)	horizontal π-complex (b)	α-agostic transition state (c)	γ-agostic propyl product (d)	β-agostic propyl product (e)	vertical π-complex (f)	horizontal π-complex (g)	α-agostic π-complex (h)	β-agostic π-complex (i)	β-agostic transition state (j)	α-agostic transition state (k)	δ-agostic pentyl product (l)	γ-agostic pentyl product (m)	β-agostic pentyl product (n)
C1	0.0	−85.8	−83.3	−50.5	−113.1	−129.1	−176.7	−172.2	−174.7	−168.3	−134.1	−157.5	−225.8	−229.4	−238.5
C2	−25.0	−91.6	−90.0	−58.4	−121.3	−138.2	−183.3	−181.6	−180.5		−139.6	−164.0	−236.3	−239.2	−251.3
C3	−30.0	−96.1	−95.3	−64.5	−131.9	−150.1	−181.2	−178.6	−182.2	−169.6	−136.7	−168.0	−239.4	−246.8	−260.1
C4	−57.5	−92.6	−94.3	−65.9	−139.6	−164.5	−184.1		−180.2		−137.0	−166.2	−249.4	−253.6	−274.5
C5[a]	−103.7	−92.4	−94.8												
C6	−1.0	−93.1	−86.9	−54.2	−115.6	−128.6	−186.0	−179.4	−179.8	−175.3	−142.0	−154.0	−227.6	−231.2	−239.3
C7	−24.0	−101.7	−99.3	−65.2	−127.7	−147.0	−190.6	−185.6	−188.6		−142.9	−170.6	−240.2	−243.8	−257.6
C8	16.0	−86.7	−76.6	−42.4	−104.5	−111.9	−179.9	−171.1	−176.1	−166.9	−136.3	−152.1	−216.3	−220.1	−222.7
C9	−21.8	−91.9	−86.3	−57.3	−121.1	−132.8	−173.0	−166.7	−172.0		−125.7	−146.2	−228.4	−234.2	−242.6
C10	−31.6	−105.9	−102.9	−70.1	−136.4	−155.0	−195.0		−191.6		−146.0	−173.1	−250.0	−251.8	−265.8
C11[b]	−62.8	−103.8	−102.3	−70.9	−140.7	−159.6	−189.7	−186.0	−185.3		−144.8	−174.3		−267.9	
C12	−20.6	−98.2	−93.7	−62.8	−127.4	−141.6	−186.1	−181.0	−184.4	−171.8	−137.6	−159.8	−239.0	−242.0	−251.6
C13[a]	−105.9	−94.2	−94.1												
C14	−18.6	−99.6	−94.3	−62.8	−126.5	−145.0	−191.3	−186.8	−186.4		−139.7	−167.4	−239.9	−242.8	−255.5
C15	−31.5	−96.6	−94.5	−65.4	−130.6	−142.1	−176.7		−174.6		−132.8	−152.0	−237.1	−242.9	−252.8
C16	−31.6	−97.0	−94.6	−66.0	−130.8	−143.9	−176.8		−175.2		−132.3	−152.9	−237.6	−243.5	−253.9
C17	−32.7	−98.1	−95.1	−66.3	−131.5	−144.2	−177.7		−176.6		−133.1	−154.2	−238.1	−243.8	−254.2
C18	−35.1	−97.2	−95.5	−67.0	−132.0	−145.1	−176.9		−173.8		−133.1	−153.1	−239.2	−244.3	−255.2
C19	−17.3	−99.0	−94.6	−62.9	−124.4	−142.6	−188.8	−184.5	−186.8		−137.9	−169.2	−236.6	−239.9	−253.2
C20	−38.5	−102.5	−104.3	−70.1	−136.0	−148.7	−185.9	−186.9	−189.7		−140.1	−173.8	−238.0	−253.2	−267.2
C21	−123.2	−129.9	−122.3	−99.3	−173.7	−196.8	−196.2	−200.1	−205.1		−151.3	−189.5	−276.9	−274.1	−304.6
C22	−16.2	−96.4	−91.3	−59.8	−124.1	−137.6	−184.3		−182.3		−135.5	−157.0	−235.3	−238.8	−247.9
C23[c]	−0.1	−96.0		−50.7	−114.9	−123.1	−189.5		−184.5	−170.0	−139.2	−150.4	−224.7	−230.2	−233.6
C24[c]	−2.9	−98.3		−52.6	−116.6	−124.7	−191.3		−185.8		−140.5	−159.3	−226.5	−231.1	−235.4
C25	−49.0	−119.5	−117.9	−82.9	−150.8	−164.1	−206.3	−208.1	−205.4		−145.9	−178.0	−257.5	−263.9	−274.3
C26	−28.3	−91.8	−87.3	−57.9	−127.2	−143.0	−172.1	−171.7	−176.5		−132.4	−160.8	−234.8	−241.1	−252.9
C27[d]	−94.1	−139.3	−141.1	−109.7	−178.6	−195.6		−220.6	−221.2		−169.1	−207.6	−288.9	−292.0	−306.2
C28	−102.1	−140.2	−138.9	−108.2	−188.5	−208.0	−215.7	−207.3	−220.9		−166.1	−200.1	−293.2	−299.7	−317.0
C29[d]	−54.9	−99.5	−90.9	−62.4	−138.4	−163.2		−197.1	−196.1		−149.6	−185.3	−250.6	−262.9	−274.8
C30	−26.6	−106.0	−98.9	−65.6	−129.2	−139.4	−197.4		−193.9	−176.7	−147.0	−164.2	−237.2	−242.8	−249.2
C31	−38.2	−98.6	−99.8	−70.3	−138.4	−146.2	−172.0	−175.0	−182.9		−134.8	−164.6	−243.6	−249.8	−252.4
C32	−20.7	−110.7	−102.8	−68.2	−133.7	−139.8	−199.7		−197.1	−174.4	−148.7	−174.5	−242.4	−247.1	−250.1
C33	−105.8	−146.8	−150.5	−115.0	−183.1	−208.5	−230.3	−230.9	−232.0		−177.4	−219.4	−300.2	−302.0	−317.3
C34	−30.9	−115.4	−110.0	−73.5	−141.8	−149.2	−204.5		−204.5		−146.4	−178.0	−250.3	−255.2	−259.2
C35	−43.9	−123.7	−118.0	−81.1	−151.7	−160.6	−212.3	−204.5	−212.3		−149.7	−184.9	−260.6	−265.1	−270.7
C36	−50.6	−118.6	−113.3	−78.7	−147.6	−156.7	−196.4		−203.3		−144.1	−175.2	−254.0	−259.0	−265.6
C37	−75.3	−118.9	−122.6	−92.5	−166.4	−177.4	−196.1	−197.3	−201.1		−147.9	−182.4	−271.7	−277.1	−286.6
C38	−58.9	−126.2	−123.7	−89.9	−160.0	−173.2	−214.7		−214.1		−152.7	−184.7	−268.1	−271.7	−283.2
C39	−35.2	−118.1	−112.4	−74.3	−141.9	−148.0	−200.2	−194.4	−203.1		−145.0	−174.8	−253.9	−254.8	−258.3
H1	−21.4	−94.9	−92.5	−61.9	−126.5	−141.6	−179.9	−178.5	−181.0		−130.6	−164.6	−237.5	−239.9	−251.9
H2	−20.3	−99.8	−97.0	−65.6	−127.2	−141.8	−189.6		−186.6		−141.6	−171.6	−238.3	−241.0	−251.9
H3	−40.2	−111.8	−112.4	−74.7	−139.2	−153.3	−199.6	−202.3	−198.6		−149.4	−180.9	−249.1	−252.1	−263.6
H4	−63.9	−108.6	−102.7	−68.6	−137.4	−163.7	−191.0	−185.0	−193.2		−130.7	−169.6	−246.8	−249.6	−273.1
H5	−81.3	−118.4	−116.5	−78.4	−143.9	−155.7	−188.5		−176.8		−144.1	−172.8	−250.3	−264.1	−281.4
H6	−42.6	−107.6	−99.2	−59.7	−126.9	−151.4	−194.4	−185.4	−195.0		−134.7	−164.3	−239.4	−242.0	−260.9
H7	−79.1	−98.0	−110.9	−80.0	−148.2	−172.4	−170.5	−179.2	−180.0		−136.7	−172.1	−252.3	−261.7	−278.7
H8	−46.0	−110.7	−103.6	−64.5	−132.5	−155.4	−189.0		−196.3		−133.1	−166.1	−237.6	−243.1	−265.3
H9	−54.8	−111.3	−109.0	−77.8	−151.0	−171.4	−194.0		−194.3		−141.7	−180.4	−255.2	−255.3	−280.2
H10	−72.4	−149.4	−144.2	−98.1	−159.3	−179.9	−233.7		−235.0		−168.3	−202.2	−267.6	−272.8	−289.8
H11	−46.4	−111.9	−104.2	−65.5	−132.8	−157.2	−201.1		−199.9		−140.1	−169.2	−244.5	−248.2	−267.5
H12	−59.9	−116.2	−117.5	−85.7	−151.4	−163.9	−187.5		−195.0		−140.1	−178.6	−252.5	−261.6	−273.3
H13	−49.4	−114.2	−117.6	−78.9	−145.6	−160.3	−200.2		−200.8		−152.9	−183.0	−254.0	−256.8	−278.4
H14	−67.0	−135.4	−129.3	−90.0	−152.5	−172.4	−203.2		−199.0		−160.5	−194.0	−275.8	−266.2	−280.3
H15	−47.0	−119.3	−113.8	−84.6	−150.5	−164.1	−205.7		−204.5		−154.3	−180.5	−256.9	−262.9	−274.0

[e] Relative energies (ΔE) are energy differences from the catalytic intermediates to the sum of the energies of the free cationic monomethyl forms and free ethene molecules. The cationic monomethyl form of hafnocene C1 is set as a reference structure ($\Delta E = 0$). [a] Formation of the π-complex is endothermic; rest of the reaction pathway is omitted. [b] β- and δ-agostic pentyl products were not formed. Instead, the pentyl chain straightened, the phenyl substituent coordinating to the metal. The relative stability of this pentyl product −309.4 kJ/mol. [c] The horizontal π-complex rearranged to the vertical π-complex. [d] In the second ethene insertion, the vertical π-complex rearranged to the horizontal π-complex.

Table 2. Summary of the Ethene Insertion and Chain Propagation Pathways for "the Hf-Set"[e]

	ΔE_{av}	ΔE_{min}	ΔE_{max}
1st insertion: generally exothermic	−63.0	−102.6	11.6
1st insertion: vertical π-complex favored over horizontal	−2.8	−10.1	12.9
1st insertion: activation energy for chain propagation	33.0	23.1	46.2
1st insertion: formation of γ-agostic propyl product exothermic	−30.4	−50.2	−9.9
1st insertion: β-agostic propyl product favored over γ	−15.5	−26.3	−6.1
2nd insertion: vertical π-complex favored over horizontal[a]	−2.6	−9.0	8.6
2nd insertion: the favored π-complexes f and h[b] on average equal in energy	−0.1	−11.6	11.0
2nd insertion: π-complex with straight chain favored over the β-agostic one[c]	−15.4	−25.2	−8.5
2nd insertion: α-agostic TS favored over β-agostic	−28.8	−42.0	−11.2
2nd insertion: lowest activation energy for chain propagation	22.3	7.9	39.1
2nd insertion: formation of γ-agostic pentyl product exothermic	−80.7	−99.6	−68.0
2nd insertion: β-agostic propyl product favored over γ[d]	−12.3	−30.5	−2.6

[a] Twenty-seven structures included in comparison. [b] See Figure 1. [c] Eight structures included in comparison. [d] The δ-agostic pentyl product is always unfavored. [e] Relative energies are given in kJ/mol.

of the first ethene, the vertical conformer (see Figure 2a) is favored in energy, on average by 2.8 kJ/mol. In this regard, zirconocenes appear to show a different behavior. The zirconocene analogue of C1 (see Figure 1) has been previously shown to favor the horizontal conformer,[6q] whereas the C1 hafnocene reported here favors the vertical conformer. It is notable that the horizontal π-complex is necessary for the reaction to continue toward the four-centered transition state, and the general preference of the vertical π-complex in hafnocenes could slow the polymerization reaction. The four-centered transition states show α-agostic interactions (Figure 2c), from which the reaction continues to produce first the γ-agostic propyl product (Figure 2d) and, after rotation of the chain, the β-agostic propyl product (Figure 2e). The β-agostic propyl product is always favored in energy over the γ-agostic one, which has also been reported for zirconocenes.[6j,k,q,x]

Insertion of the second ethene monomer is more complex due to the various conformations of the propyl chain during the formation of the π-complex and the transition state. The conformational freedom of the propyl chain, together with the possibility of forming both vertical and horizontal π-complexes, was taken into account. As a preliminary study, all four resulting π-complexes were studied for eight hafnocenes, based on which two energetically favored conformers were applied for the rest of the hafnocenes. The two favored π-complexes are on average equal in energy, and they are illustrated in Figure 2 (f and h). The one with a straight propyl chain without agostic interactions and a vertical π-complex (f) has been previously described for zirconocenes by Petitjean et al. in a stepwise back-side mechanism[6q] and also for zirconcenes by Jensen et al. in a front-side mechanism.[6x] Here, for hafnocenes, it is produced by the back-side mechanism, suggesting that the process may be easier for hafnocenes than for zirconocenes. The other energetically favored π-complex (h) usually leads to a transition state with an α-agostic interaction from the propyl chain to the metal and a vertical π-complex, which usually form from the front-side insertion, but has also been suggested to form from back-side insertion.[6] While the two π-complexes are on average equal in energy, the latter with the α-agostic interaction is typically favored for catalysts with steric bulk.

Concerning the four-centered transition states after the insertion of the second ethene, two possibilities were taken into account. The β-agostic transition state (Figure 2j) is generally considered to be produced by the back-side mechanism, while the α-agostic transition state (Figure 2k) is mainly produced by the front-side mechanism.[6] The α-agostic transition state is always energetically favored over the β-agostic one, as has been reported also for zirconocenes.[6j,k,n–r,x] Following the transition states, there are three possibilities for the pentyl products: δ-, γ-, and β-agostic (Figure 2, l−n). The δ-agostic pentyl product is produced from the β-agostic transition state, and the γ-agostic product from the α-agostic transition state. The β-agostic pentyl product is formed after rotation of the chain and is energetically favored in all cases.

3.3. Comparison of the Hafnocenes. "The Hf-set" (see Figure 1) enables systematic analysis of the effects of ligand modification to the ethene insertion and propagation pathways. It should be noted that all calculations are performed without the presence of cocatalyst, thus representing the case of an ideal noncoordinating cocatalyst anion. As an example for the comparison of the ligand structure, the relative energies of the preferred catalytic intermediates along the ethene insertion and propagation pathways are shown in Figure 3 for four hafnocenes. These are C1, H14, C4, and C6 (see Figure 1), which enable direct comparison of changing the ancillary cyclopentadienyl (Cp) ligand to indenyl (Ind) (C1 vs H14), adding an alkyl substituent to the Cp ligand (C1 vs C4), and adding a $SiMe_2$ bridge (C1 vs C6).

The starting point in the comparison is the stability of the cationic monomethyl form of the catalyst relative to its dichloride precursor form. This is shown in the leftmost column of the graph. The relative stability of the cation serves as an indication of the feasibility of the activation step and thus has an apparent relation with the concentration of active metal centers available for the incoming monomers.[16,17] After the cationic monomethyl form, the energetically preferred catalytic intermediates along the reaction path follow in the order (a) vertical π-complex, (c) α-agostic four-centered transition state, (d) γ-agostic propyl product, (e) β-agostic propyl product, (f) vertical π-complex for the second ethene insertion with no agostic interactions, (k) α-agostic four-centered transition state for the second ethene insertion, (m) γ-agostic pentyl product, and (n) β-agostic pentyl product.

As is clear from Figure 3, the hafnocenes C1, H14, C4, and C6 basically behave in a similar way, the polymerization reaction being energetically favorable. The most significant difference between the catalysts originates from the relative stability of the cationic monomethyl form, i.e., from the feasibility of the activation step. Compared to the plain Cp ligand (C1), the relative stability of the cation is significantly increased by the Ind ligand (H14) and by the alkyl substituent (C4), but not by the $SiMe_2$ bridge (C6). The effects of the electron-rich Ind ligand and the electron-donating alkyl substituent is

(17) (a) Hortmann, K.; Brintzinger, H.-H. *New J. Chem.* **1992**, *16*, 51. (b) Janiak, C.; Lange, K. C. H.; Versteeg, U.; Lentz, D.; Budzelaar, P. H. M. *Chem. Ber.* **1996**, *129*, 1517. (c) Linnolahti, M.; Pakkanen, T. A. *Macromolecules* **2000**, *33*, 9205. (d) Möhring, P. C.; Coville, N. J. *Coord. Chem. Rev.* **2006**, *250*, 18.

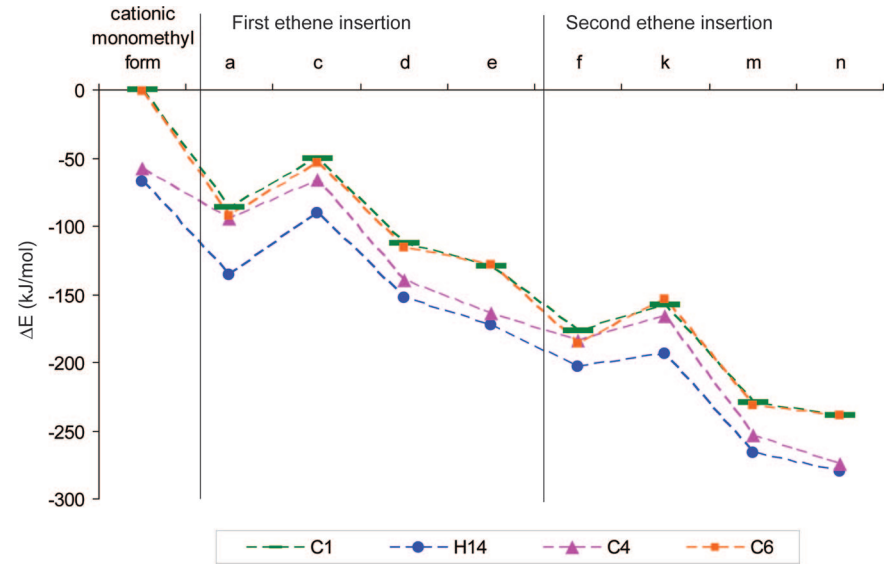

Figure 3. Comparison of ancillary ligand (C1 vs H14), ligand substituent (C1 vs C4), and bridge (C1 vs C6) in the reaction pathway including the most stable π-complex, transition state, and γ- and β-agostic product.

understandable, as the extra electrons stabilize the cation. On the other hand, the effect of bridges is mostly steric, thereby not affecting the stability of the cation.[16,17c]

Beyond the cationic monomethyl form the differences between the behaviors of the catalysts become relatively small. The energy for the formation of the first π-complex (a) is the highest for C6 with a $SiMe_2$ bridge. This is because the short bridge opens the Cp−Cp plane,[16] making the metal center more easily accessible for the ethene monomer. On the contrary, the bulky alkyl substituent of C4 makes the metal center crowded, thus resulting in the lowest energy for the formation of the first π-complex. The accessibility of the reaction center has less importance when proceeding to the transition state (c). This is due to the orientation of ethene, which in the π-complex prefers a vertical arrangement but in the transition state must be horizontal. The vertical ethene requires more space, making the steric environment due to the ligand structure more influential. This has a consequence of increasing the activation energy for the bridged catalyst (C6), while lowering it for the one with bulky alkyl groups (C4). In the γ- and β-agostic propyl products (d and e), the relative stabilities of the catalyst intermediates have returned back to about the situation before the ethene insertion, i.e., the relative stabilities of the cationic monomethyl forms (a). The differences in relative stabilities have become smaller, however. This is apparently due to the cation stabilizing agostic interactions, which are not present in the cationic monomethyl form. In other words, the role of electron-rich ligands and electron-donating substituents in stabilizing the cation is stronger when agostic interactions are present than when they are not. Insertion of the second monomer (f−n) practically reproduces the behavior of the first monomer.

The ethene insertion and chain propagation pathways calculated for "the Hf-set" enable a similar comparison for a larger number of structural variables. In the following, the behaviors of the catalysts are analyzed to single out the effects of various ancillary Cp ligands, ligand substituents, and bridging units. The analysis is based on the data given in Table 1. Graphical illustrations of the pathways, like the one shown in Figure 3, are given in Appendix 1 for each comparison.

Effect of Cp′ Ligand. The effect of the ancillary Cp′ ligand (Cp′ = any cyclopentadienyl-based ligand) is compared for cyclopentadienyl (Cp), indenyl (Ind), tetrahydroindenyl (Thind), and cyclopentadienylfluorenyl (CpFlu). The effect of changing Cp to Ind can be figured out by comparing C1 with H14 and C6 with H15. Changing Cp to the more electron-rich Ind greatly stabilizes the cationic monomethyl form, the other changes being marginal compared to that. Concerning the other changes, the formation of the π-complex is more exothermic for Cp, because of the increased steric bulk introduced by Ind. Generally, the activation energy for the reaction to proceed from the π-complex to the γ-agostic product is higher for Cp. This is apparently contributed by the reduced steric requirements in the transition state, where the orientation of the ethene monomer is always horizontal. The formations of the γ- and β-agostic propyl and pentyl products are more exothermic for Ind. Nevertheless, the differences between Cp and Ind have decreased compared to the initial state of the cationic monomethyl form, which lacks the cation-stabilizing agostic interactions.

The effect of changing Cp to CpFlu can be seen by comparing C8 to C34. The behavior of CpFlu with respect to Cp is very similar to the Cp vs Ind case described above. The cation-stabilizing influence of CpFlu is practically identical to that of Ind and is clearly the dominant effect. As with Ind, the formation of the π-complex is less exothermic for CpFlu. Activation energies from the π-complex to the γ-agostic product are about the same, while the formations of γ- and β-agostic propyl and pentyl products are more exothermic for CpFlu. The differences between Cp and CpFlu become smaller for catalyst intermediates with agostic interactions.

Comparison between C25 and C26 reveals the effect of changing Ind to Thind. Saturation of the six-membered ring of the ligand makes Thind a worse electron donor than Ind. As a consequence, the cationic catalyst intermediates become destabilized, dominating also this comparison. The difference is highest for the π-complex, because of the larger steric hindrance of Thind. Unlike with the Cp vs Ind and Cp vs CpFlu comparisons, the differences do not become smaller in the catalytic intermediates later than the cationic monomethyl form. Rather, they seem to increase slightly in favor of Ind. This behavior appears to originate from the agostic interactions being stronger for Ind.

Effect of Ligand Substituent. The influence of adding a variable number of methyl groups to the Cp ring of the ancillary Cp′ ligand can be analyzed by comparing C1 to C3, C6 to C22

Table 3. Summary of the Effects of Ligand Modifications of Hafnocenes on Ethene Insertion and Chain Propagation[a]

	typically increased by	typically decreased by	max.	min.
relative stabilities of the catalytic intermediate products	large aromatic Cp′ ligands, electron-donating substituents	electron-withdrawing substituents, short bridges	C33	C8
feasibility of π-coordination	short bridges	bulky substituents	C8	H7
activation energy for chain propagation	short bridges	large number of ligand substituents	C23	H7

[a] The catalysts representing the maxima and the minima are taken from the second ethene insertion.

and C15, C12 to C18, H6 to H4 and H7, H11 to H9 and H12, and C34 to C39. Generally, the stabilities of the cationic catalyst intermediates increase as a function of the electron-donating methyl substituent. Addition of the methyl groups leads to steric congestion of the active reaction center. This is best seen in the π-complex formation energies, which decrease as a function of the number of methyl groups. The effect is stronger for the second ethene insertion, because of the possibility for two π-complexes, one with α-agostic interaction and the other without it. Generally, the complexes with large steric bulk prefer α-agostic π-complexes. The combination of a phenyl substituent in the indenyl ligand and methyl substituents in the Cp ligand (see H4, H6, H7, H9, H11, H12) leads to a particularly strong effect. As a consequence, addition of methyl groups in these complexes destabilizes the π-complexes but stabilizes the transition state with respect to the π-complex, thereby strongly lowering the activation energy for the chain propagation.

The influence of alkyl substituents larger than methyl can be analyzed by comparing C1 to C2, C4, C20, and H1, C32 to C31, H6 to H8, and H11 to H13. Generally, the effects of the larger alkyl substituents are the same as those of methyl groups, while somewhat larger: They (1) stabilize the cationic catalyst intermediates, (2) destabilize the π-complexes, (3) stabilize the transition states, and thereby (4) lower the activation energies for chain propagation. The effects are stronger for the Ind than for the Cp ligands.

The influences of aromatic substituents can be figured out by comparing C1 to C11 and C21, and H14 to C27, C28, H5, H10, and C33. Aromatic substituents strongly stabilize the cations. The steric bulk introduced by the substituents destabilizes the π-complexes and lowers the activation energies. The effects, however, are dependent on the position of the substituent, which will be analyzed below. It is notable that the aromatic ring of the benzyl-substituted C11 interacts with the metal center, thus providing further stabilization for the cation. This effect has been previously observed for benzyl-substituted zirconocenes.[18] Likewise, the chlorine of C5 coordinates to the metal center, in which case the coordination is so strong that it prevents any further polymerization reactions.

The effect of the position of the phenyl substituent attached to the Ind ligand can be seen by comparing H6 to H11, H4 to H9, H7 to H12, H8 to H13, and C28 to H5 and H10. The relative stabilities of cationic monomethyl forms mostly increase in the order 4-phenyl < 3-phenyl < 2-phenyl. The lowest relative stability obtained with the 4-phenyl substituents is due to the phenyl substituent being attached to the six-membered ring of the Ind ligand, where the electronic stabilization of the cation is weaker than when attached to the five-membered ring. On the other hand, the 4-phenyl substituent stabilizes the π-complexes with respect to the corresponding 3- and 2-phenyl substituents. Apparently, the steric congestion of the reaction site is lower for the 4-substituent due to their longer distance from the reaction center. As noted previously, the steric congestion is less significant in the transition state, and therefore the activation barrier is the highest with the 4-benzyl substituents. Overall, the feasibility of the polymerization reactions appears to increase in the order 3-phenyl < 4-phenyl < 2-phenyl.

The effects of electron-withdrawing fluorine substituents are seen by comparing C28 to C29. As expected, the electron-withdrawing substituents strongly destabilize the cationic catalytic intermediates. This is clearly the dominant effect of the substituent, the chain propagation pathway showing only small differences between the two catalysts.

Effect of Bridge. The influence of adding bridges between the ancillary Cp′ ligands can be clarified by comparing C1 to C6, C7, C8, C10, C13, C14, C19, C23, and C24, H14 to H15, C25, and C32, H1 to H2, and H6 to H3. The most influential structural feature of the bridge is its size. Short bridges, in particular one-atom bridges, usually destabilize the cationic monomethyl form. The formation of the π-complexes is the most exothermic with short bridges, which strongly open the Cp′−Cp′ plane angles, thereby making the coordination site more accessible for the incoming monomer. The effects of long bridges are typically the reverse of the effects of short bridges. They stabilize the cations but make the coordination site less accessible due to small Cp′−Cp angles.[16] The highest relative stability among the bridges is obtained by C13, but it is due to coordination between the metal center and the oxygen atom of the bridge. Nevertheless, the overall effects of the bridges are small if compared to the effects of aromatic substituents, for instance. It is notable that the behaviors of the two very common bridges $Si(CH_3)_2$ and $(CH_2)_2$ are practically equal all the way along the reaction pathway (see H15 vs C25).

3.4. Summary of Ligand Effects. The main effects of ligand modifications on ethene insertion and chain propagation, as analyzed above, are summarized in Table 3. Generally, the polymerization reactions appear to proceed smoothly, the differences between the catalysts being dominated by the relative stabilities of the catalytic intermediate products. The catalytic intermediates are mostly stabilized by large aromatic Cp′ ligands and electron-donating substituents, possibly resulting in an increased concentration of active reaction centers in the polymerization systems. The relative stabilities of the catalytic intermediates of the hafnocenes correlate well with those reported previously for zirconocenes,[17c] suggesting the zirconocenes and hafnocenes to show similar polymerization behavior as a function of ligand structure. For comparison, aromatic Cp′ ligands and electron-donating substituents typically provide enhanced polymerization activities for zirconocenes.[3,19] On the other hand, the effect of electron-withdrawing substituents is the reverse, destabilizing the catalytic intermediate products. Also short bridges destabilize the cations.

Concerning the other changes along the chain propagation pathway, the feasibility of ethene π-coordination together with activation energies for chain propagation show clear trends and seem to be linked to each other. The feasibility of π-coordination

(18) Aitola, E.; Surakka, M.; Repo, T.; Linnolahti, M.; Lappalainen, K.; Kervinen, K.; Klinga, M.; Pakkanen, T.; Leskelae, M. *J. Organomet. Chem.* **2005**, *690*, 773.

(19) Moehring, P. C.; Coville, N. J. *J. Organomet. Chem.* **1994**, *479*, 1.

is typically increased with reduced steric crowding around the reaction center. Hence, stabilities of the π-complexes relative to the other catalytic intermediates are mostly improved by short bridges, which open up the Cp′−Cp′ plane angles.[1–6] Bulky substituents usually complicate the formation of the π-complex by introducing steric hindrance for the monomer approaching the reaction center. A feasible π-coordination typically indicates high activation energy for chain propagation. This is because of reduced impact of steric crowding when proceeding from the π-complex to the transition state. The activation energies for chain propagation are usually increased by short bridges together with substituents on the 4-position of the indenyl ligand and decreased by a large number of ligand substituents. It is notable, however, that the activation energies are low for all studied hafnocenes, in the range 8−46 kJ/mol at the B3LYP level of theory.

4. Conclusions

The influence of the ligand framework of hafnocene catalysts on ethene insertion and chain propagation pathways was systematically studied for 54 catalyst complexes. The chain propagation reactions were studied for insertions of the first and the second monomer, and consequently, the structures of altogether 15 catalytic intermediates along the reaction pathway were optimized by the hybrid density functional B3LYP method. The preferred polymerization pathways were determined and analyzed as a function of the ligand structure of the catalysts, with a particular focus on the effects of various ancillary Cp′ ligands, ligand substituents, and bridging units.

While both the feasibility of the π-coordination and the activation energies for chain propagation show apparent and systemic behavior, clearly the dominant difference between the catalysts is the relative stabilities of their catalytic intermediate products. This can be rationalized to the relative stability of the cationic monomethyl form, produced in the activation step, as the relative stabilities of all other catalytic intermediates usually follow the same trends. The stability of the cation is mostly increased by aromatic Cp′ ligands together with electron-donating substituents and mostly decreased by electon-withdrawing susbtituents. Concerning the other changes along the reaction pathway, the feasibility of the π-coordination and the activation energies for chain propagation are directly linked to the steric enviroment of the active reaction center. Overall, the obtained trends are expected to provide insight for the behavior of hafnocene polymerization catalysts and to be of use in further catalyst development.

Supporting Information Available: Appendix 1 and coordinates of all optimized structures. This material is available free of charge via the Internet at http://pubs.acs.org.

OM800050D